

Interfacial disorder in InAs/GaSb superlattices

By M. E. TWIGG†, B. R. BENNETT†, P. M. THIBADO‡§,
B. V. SHANABROOK† and L. J. WHITMAN‡

† Electronics Science and Technology Division, Naval Research Laboratory,
Washington, DC 20375-5347, USA

‡ Chemistry Division, Naval Research Laboratory, Washington, DC, USA

§ Department of Physics, University of Arkansas, Fayetteville, Arkansas, USA

[Received 13 January 1997 and accepted in revised form 11 April 1997]

ABSTRACT

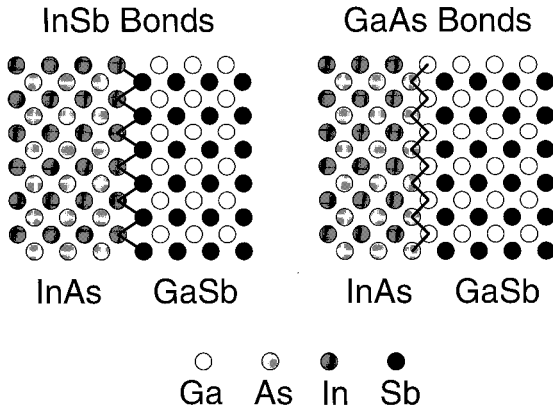
We have addressed the question of interfacial disorder in InAs/GaSb superlattices (SLs) grown by molecular-beam epitaxy using high-resolution transmission electron microscopy, Raman spectroscopy, X-ray diffraction, and *in-situ* scanning tunnelling microscopy (STM). Our analysis indicates that InSb-like interfaces have a roughness of 1 monolayer (ML), for a SL grown on a GaSb buffer layer. For GaAs-like interfaces, however, the interface roughness is found to be 2 ML when the SL is grown on a GaSb buffer. For SLs grown on an InAs buffer, the roughness of GaAs-like interfaces (3 ML) is also greater than that of InSb-like interfaces (2 ML). These results suggest two general observations. The first is that GaAs-like interfaces are rougher than InSb-like interfaces. This difference may be due to the high surface energy of GaAs compared with InSb or to differences in surface kinetics. These observations are supported by *in-situ* STM results showing that the growth front surface morphology, for both GaSb and InAs layers, is rougher for GaAs-like interfaces than for InSb-like interfaces. We have also found that interface roughness is greater for an InAs/GaSb SL grown on an InAs buffer layer than for the same SL grown on a GaSb buffer layer. This difference in interface roughness may arise because InAs SL layers are in tension when grown on a GaSb buffer layer, whereas GaSb SL layers are under compression when grown on an InAs buffer layer.

§ 1. INTRODUCTION

For advanced opto-electronic devices, such as infrared detectors based on an InAs/Ga_{1-x}In_xSb superlattice (SL), the deleterious effects of interface roughness are particularly important. In these device structures the thickness and composition of the layers are tailored to achieve the desired bandgap (Smith and Mailhiot 1987, Miles *et al.* 1990, Waterman *et al.* 1993). The effects of interfacial disorder are expected to be deleterious to the functioning of most device structures based on a SL. In the case of an infrared detector, interfacial disorder would alter the band structure of the device, since this band structure is due, in large part, to the SL periodicity. In addition, interfacial disorder may reduce carrier mobility (Tuttle *et al.* 1990).

The novel properties of a short-period semiconductor SL depend on the ability to grow thin layers with thickness and composition controlled on an atomic scale. This degree of control can be achieved by molecular-beam epitaxy (MBE). The challenge, however, is in controlling the structure of a strained SL given the large volume fraction consisting of interfaces. In forming an interface, the growth temperature

Fig. 1



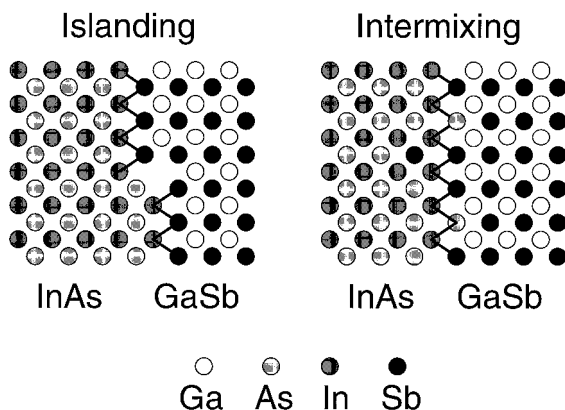
Interfacial bonding configuration for InSb-like and GaAs-like bonds at the InAs–GaSb interface as viewed along the [100] direction.

needs to be sufficiently high (and the growth rate sufficiently low) to allow the adatoms arriving on the surface to assemble into a flat monolayer before the next monolayer begins; at the same time the temperature cannot be so high as to promote diffusion below the surface and into the bulk. At each thermal extreme there is a potential complication. At too low a temperature, the deposited monolayer may not have the opportunity to distribute itself smoothly (and thereby to reduce surface roughness). At too high a temperature, intermixing may occur at the interface. All aspects of interfacial disorder are usually undesirable in opto-electronic devices. Interfacial roughness, the result of too low a growth temperature, is thought to have a deleterious effect on carrier mobilities (Hoffman *et al.* 1993). Interfacial intermixing, due to too high a growth temperature, can alter the carefully engineered bandgap (Chow *et al.* 1992).

By the term *interfacial disorder*, we mean any deviation from an interface that is perfectly smooth and compositionally abrupt. In fig. 1 we show the two possible configurations for a perfectly ordered InAs/GaSb interface: one consisting of InSb-like bonds and the other consisting of GaAs-like bonds. In large part, there are two major components to interfacial disorder (as shown in fig. 2). The first component, interfacial roughness, is due to the formation of steps and islands which in turn lead to uneven coverage of the heteroepitaxial surface (Ourmazd *et al.* 1989, Warwick *et al.* 1990, Gammon *et al.* 1991, Grigorieff *et al.* 1993). The second component, interfacial diffuseness, is due to mixing driven by both stochastic processes (simple diffusion) and differences in bonding energies (exchange reactions) (Schmitz *et al.* 1995). Strain may also play a role in diffusion kinetics. Because the chemical potential increases with increasing strain, and atomic diffusion follows the gradient of the chemical potential, strain at the interface may undermine interfacial stability and promote interfacial diffuseness (Moison *et al.* 1991, Bennett *et al.* 1996).

The precarious balance that must be maintained in MBE growth may also be undermined by the complexities of heteroepitaxy. Because heteroepitaxy inevitably leads to growing a monolayer of one lattice parameter and binding energy upon a surface with a different lattice parameter and binding energy, one is faced with the

Fig. 2

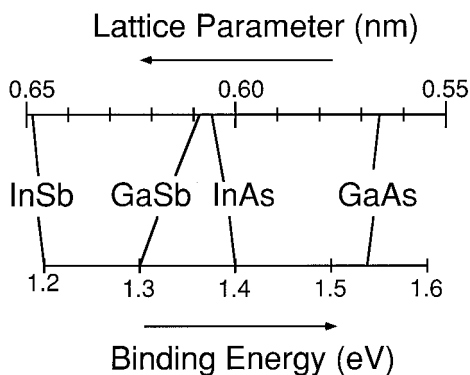


Interfacial bonding configuration for InSb-like interfaces perturbed by roughness and intermixing as viewed along the [100] direction.

problem of maintaining at least two different kinds of surface in equilibrium while growing the metastable film. The first constituent may be easily deposited at a given temperature and growth rate, with the surface in equilibrium over the course of the growth and the bulk kinetics held in abeyance. The second constituent, may, however, be more strongly bonded than the first constituent, so that reduced surface diffusion occurs and therefore the surface is not able to maintain equilibrium during growth (Copel *et al.* 1989). Differences in lattice parameter and the strain that accompanies this difference may also prevent the formation of large flat terraces on the surface.

The existence of a wide range of binding energies among the adatoms forming a heterostructural interface enhances the likelihood of exchange reactions and contributes to interfacial diffuseness. In fig. 3, we show the range of binding energies and

Fig. 3



Range of lattice parameters and binding energies for InSb, GaSb, InAs and GaAs, the four possible cation–anion bonding configurations of the InAs/GaSb system.

lattice parameters for the constituents of the InAs/GaSb heteroepitaxial growth system (Yano *et al.* 1991). This wide range in binding energies and lattice parameters is likely to frustrate any attempt to achieve the desired layer by-layer growth that is necessary for perfect epitaxy (Wang *et al.* 1995). One might expect for GaAs (or InAs) on GaSb to present more of a problem than for InSb (or GaSb) on InAs, since the antimonides have lower binding energies than the arsenides. The energy of a given surface might then be reduced by the exchange of a surface As atom with a subsurface Sb atom. Therefore exchange reactions would tend to occur when arsenides are grown on antimonides.

The nature of the growth surface itself may contribute to the difficulties in establishing a smooth and abrupt heteroepitaxial interface. Even when the first monolayer can be grown under equilibrium conditions and thereby establish two-dimensional (2D) growth (owing to the low surface energy of the deposited layer relative to the substrate), we are still faced with the problem of three-dimensional (3D) growth occurring as the second or third monolayer goes down. This transition from 2D to 3D growth in heteroepitaxy, known as Stranski–Krastinov growth, is predicted by equilibrium thermodynamics (Bauer 1958, Snyder *et al.* 1993). The formation of 3D islands, of course, is a source of interfacial roughness.

A proper understanding of the configuration of a heteroepitaxial interface should begin with the morphology of the growth surface. Recent observations using *in-situ* scanning tunnelling microscopy (STM) suggest aspects of the growth surface morphology that had not been anticipated by earlier models (Thibado *et al.* 1996). In some cases, heteroepitaxial strains may need to be relieved by the formation of vacancy lines between adjacent 2D islands (Chen *et al.* 1994, Priester and Lannoo 1995). There is also the problem of growing on top of a reconstructed surface. In the case of GaAs (Heller *et al.* 1993) and InAs (Bressler-Hill *et al.* 1994) an anion-terminated (100) surface is capable of reconstructing in such a way that the arsenic coverage is only 0.5 ML. On the other hand, GaSb(100) surfaces are capable of reconstructing such that the surface layer consists of as much as 1.7 atomic layers of antimony (Franklin *et al.* 1990). In either case, the question arises as to how a proper interface would be formed upon a reconstructed surface, given a surplus or deficit in the number of anions per unit area covering the surface.

§ 2. CONTROL OF INTERFACIAL BONDING

Given the requirement that the arriving adatoms must evenly distribute themselves across the surface, one would do well to consider a growth procedure which allows the surface atoms to assemble into an equilibrium configuration. One possible growth procedure for achieving this goal is migration-enhanced epitaxy (MEE), where one alternates between the deposition of cation and anion monolayers (Horikoshi *et al.* 1986). By depositing the cations as a separate monolayer, they are allowed to diffuse atomically over an anion-terminated surface before the next layer of anions bonds to the cations and reduces the diffusion rate. Furthermore, this growth procedure may also reduce the intermixing because it allows the formation of a complete cation monolayer prior to the deposition of the anion overlayer. This cation monolayer is thought to serve as a buffer between the subsurface anion monolayer and the subsequent anion overlayer. Because such a cation monolayer would prevent exchange reactions involving the anion layers that it separates, we speak of this cation monolayer as a ‘cation firewall’ (Twigg *et al.* 1995a,b).

Using MEE at the interfaces, we grew 40-period SLs with nominal structures of 8 monolayers (ML) InAs and 12 ML GaSb. These structures were grown on a 1 μm buffer of either GaSb or InAs on a semi-insulating GaAs(100) substrate. The growth temperature, measured by infrared transmission thermometry (Shanabrook *et al.* 1992) was 400°C. Other growth details have been given by Bennett *et al.* (1993).

In order to achieve a better understanding of local interface abruptness, InAs/GaSb SLs were also grown on a 0.1 μm GaSb buffer layer on a GaSb(100) substrate. For these samples, the GaSb buffer was grown at 500°C (a suitable temperature for achieving a smooth GaSb surface) with growth interrupts. During the growth interrupts, we observed an increase in the specular reflection high-energy electron diffraction (RHEED) intensity with time, indicating the formation of large, atomically flat terraces on the surface. Following the completion of the buffer layer, the temperature was reduced to 400°C and the SL was grown. (The formation of the large terrace structures during the growth interrupt is also verified by the observation of strong RHEED oscillations when GaSb was grown on GaSb at 400°C.)

Recent work by Bennett *et al.* (1993) and Shanabrook *et al.* (1993) have addressed the question of interfacial integrity in InAs/GaSb superlattices. According to the X-ray diffraction results of Bennett *et al.* the MEE growth technique results in well defined SLs. They concluded that interfacial control during growth resulted in a close correspondence between the intended composition and the actual composition for each SL.

Shanabrook *et al.* (1993) and Shanabrook and Bennett (1994) identified the bonding at the interface through the use of Raman spectroscopy. Planar vibrational modes, associated with the GaAs-like interfaces occurring in InAs/GaSb superlattices, have been shown to be highly localized and therefore sensitive to the structure of the interface (Sela *et al.* 1992). Furthermore, a systematic shift in wavenumber is observed as the interface bond type is altered from completely InSb-like to completely GaAs-like. This shift is also in accord with the model of the vibrational properties of the $\text{As}_x\text{Sb}_{1-x}$ interface (Shanabrook *et al.* 1993). A systematic shift is also seen in the position of the X-ray peaks for these samples. One strength of the Raman technique in this case is that the GaAs-like interface gives rise to a phonon mode that is easily observed in vibrational spectra. Because this feature is absent from the Raman spectra for SLs with only InSb-like interfaces, we conclude that this growth procedure provides a high degree of order in InSb-like interfaces of these SLs. Unfortunately, the InSb-like peak in Raman spectra is significantly weaker, making it more difficult to judge the degree of order for GaAs-like interfaces. An important addition to the type of information that can be obtained from Raman spectra was reported by Lyapin *et al.* (1994, 1995). Specifically, they showed that under particular polarization conditions the vibration properties of the top and bottom interfaces can be studied independently. Using this technique, Lyapin *et al.* determined the growth sequence in metal-organic vapour phase epitaxy (MOVPE) that allowed abrupt GaAs-like or InSb-like interfaces to be formed.

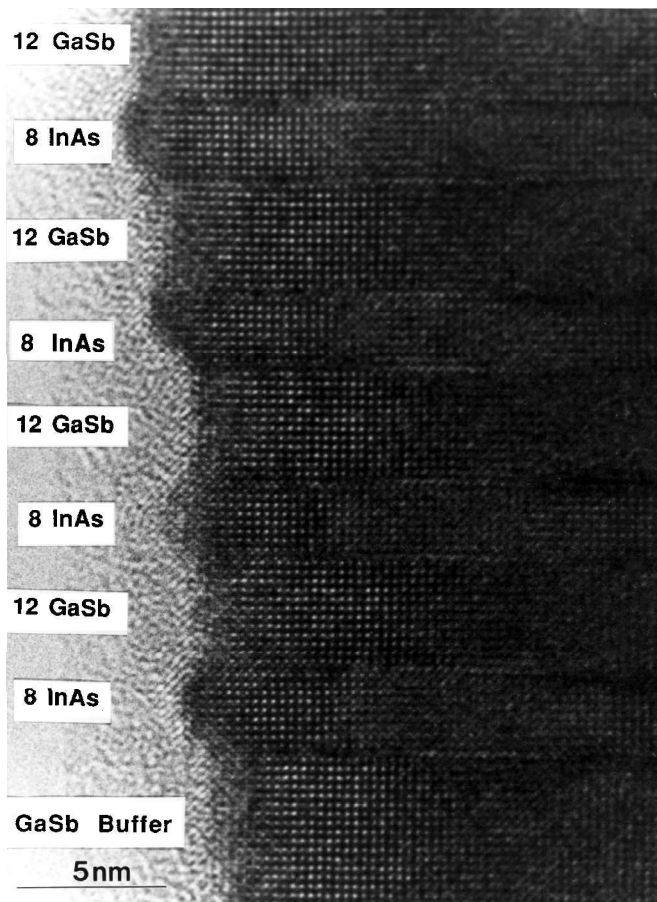
§ 3. USING HIGH-RESOLUTION TRANSMISSION ELECTRON MICROSCOPY TO STUDY INTERFACIAL DISORDER

In order to use high-resolution transmission electron microscopy (HRTEM) to measure changes in composition, such as those occurring at an interface, one needs to be able to image along a zone axis that includes reflections which are particularly

sensitive to changes in atomic number. From a simple geometrical point of view, imaging with the electron-beam direction parallel to the $[001]$ zone axis allows one to view the cations and anions in separate columns (as shown in fig. 1), thereby allowing one atomic species to be distinguished from another. The $\{200\}$ reflections of the $[001]$ zone axis are particularly useful because the strength of each $\{200\}$ reflection is proportional to the difference between the cation and anion scattering factors (Ourmazd *et al.* 1990). Therefore a $\{200\}$ reflection is strong for zincblende materials with a large difference between the atomic numbers of cation and anion, such as InAs or GaSb, the components of our SL layers. Similarly, $\{200\}$ reflections would be expected to be weak for zincblende materials with a small difference between the atomic numbers of cation and anion such as GaAs or InSb, which are responsible for the bonding at InAs–GaSb interfaces (Twigg *et al.* 1994).

An example of this imaging approach is shown in fig. 4. This image was recorded at 300 kV on a Hitachi H-9000UHR HRTEM instrument with a top-entry

Fig. 4



HRTEM image of cleaved sample taken from an InAs/GaSb SL grown on GaSb(100). The image was recorded at a defocus of 60 nm.

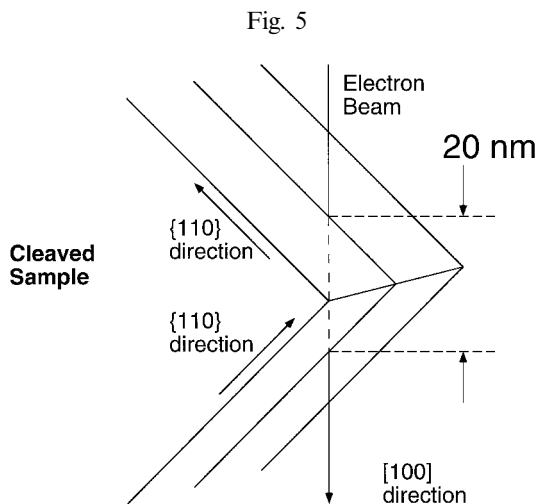


Diagram showing imaging of cleaved sample. Cleavage occurs along $\langle 110 \rangle$ directions. The sample is then mounted so that the electron beam direction is $[001]$.

goniometer and a Scherzer resolution of 0.19 nm. It should be noted that imaging InAs/GaSb heterostructures at 400 kV promotes electron-beam damage, whereas imaging at 300 kV appears free from this drawback (Murgatroyd *et al.* 1995). The sample used in making this specimen was grown on a GaSb(100) substrate, cleaved along two intersecting $\langle 110 \rangle$ directions, and then mounted in the $[100]$ cross-sectional transmission electron microscope configuration (Thoma and Cerva 1991a). A diagram of a cleaved sample is shown in fig. 5. It should be noted that InAs/GaSb heterostructures grown on GaAs(100) substrates do not appear to survive the cleaving process. An inspection of such samples in the transmission electron microscope reveals that the SL shears off the top of the sample when cleaved. In general, it seems that the cleaving process works well only when the epitaxial layer is similar to the substrate. For this reason, samples consisting of InAs/GaSb heterostructures grown on GaAs(100) were ion milled at liquid-nitrogen temperature.

3.1. HRTEM contrast of InAs/GaSb superlattices

The contrast of a HRTEM image can be controlled by selecting the thickness of the sample and the objective lens defocus. In particular, these imaging parameters can be tuned to accent the contribution of the $\{200\}$ reflections of the $[001]$ zone axis for a zincblende crystal lattice (shown in fig. 6). Applying nonlinear imaging theory (Thoma and Cerva 1991a,b), we used multislice simulations to calculate the $\{200\}$ contribution to the intensity at the cation site for both GaSb and InAs (Stadelmann 1987). As shown in fig. 7(a), for GaSb with a sample thickness in the vicinity of 15 nm, the $\{200\}$ contribution to the image intensity at the gallium site is strongly negative at a defocus (i.e. underfocus) value of 20 nm, and strongly positive at a defocus value of 60 nm. For a InAs sample 15 nm thick (as shown in fig. 7(b)), the $\{200\}$ contribution to the intensity at the indium site is strongly positive at a defocus of 20 nm while strongly negative at a defocus of 60 nm. For both GaSb and InAs, the $\{200\}$ contrast is greatest for samples of thickness in the neighbourhood of 15 nm.

Fig. 6

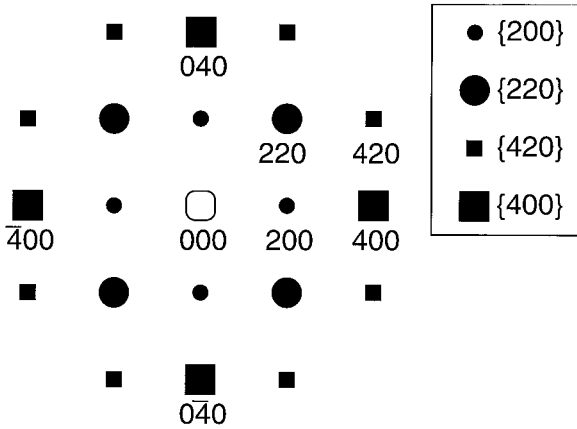
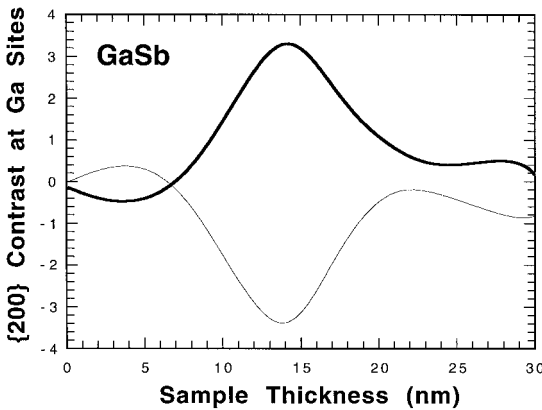


Diagram showing $[001]$ zone-axis reflections and spatial frequencies for a zincblende crystal such as InAs, GaSb, GaAs or InSb.

For GaAs and InSb, however, the $\{200\}$ contribution to the intensity at the cation sites is small, as shown in figs. 7(c) and (d) respectively. This small contribution is in accord with the small $\{200\}$ scattering factors for GaAs and InSb, where the difference between the group III and group V scattering factors (and atomic numbers) is small. Similarly, the contribution of $\{200\}$ anion contrast can also be calculated from nonlinear imaging theory. It should be noted that, at a defocus of 60 nm, the interpretation of the image is in accord with simple intuition: atomic columns corresponding to small atomic numbers (i.e. gallium and arsenic) appear bright; atomic columns corresponding to large atomic numbers (i.e. indium and antimony) appear

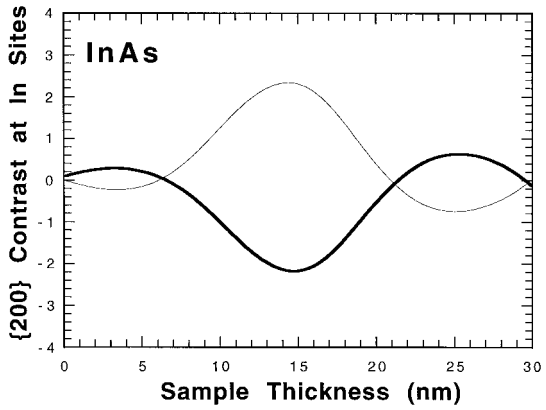
Fig. 7



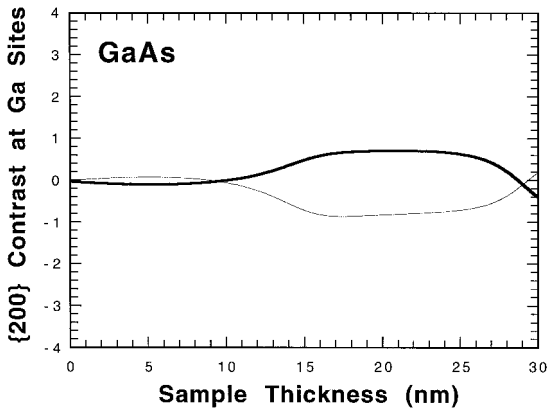
(a)

Intensity of (200) spatial frequency as a function of sample thickness for two different values of the defocus Δf (—), for (a) GaSb, (b) InAs, (c) GaAs and (d) InSb: $\Delta f = 20$ nm for the fine curve; $\Delta f = 60$ nm for the bold curve.

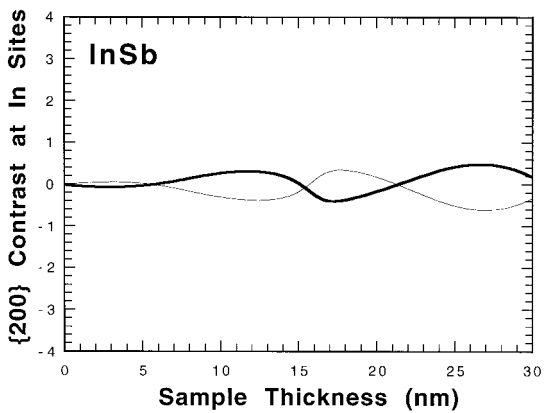
Fig. 7



(b)

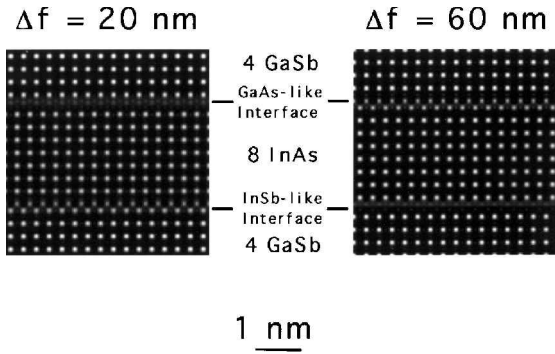


(c)



(d)

Fig. 8



Simulation of HRTEM images of abrupt InSb-like and GaAs-like interfaces for the InAs/GaSb system for two different defocus conditions $\Delta f = 20$ nm and $\Delta f = 60$ nm.

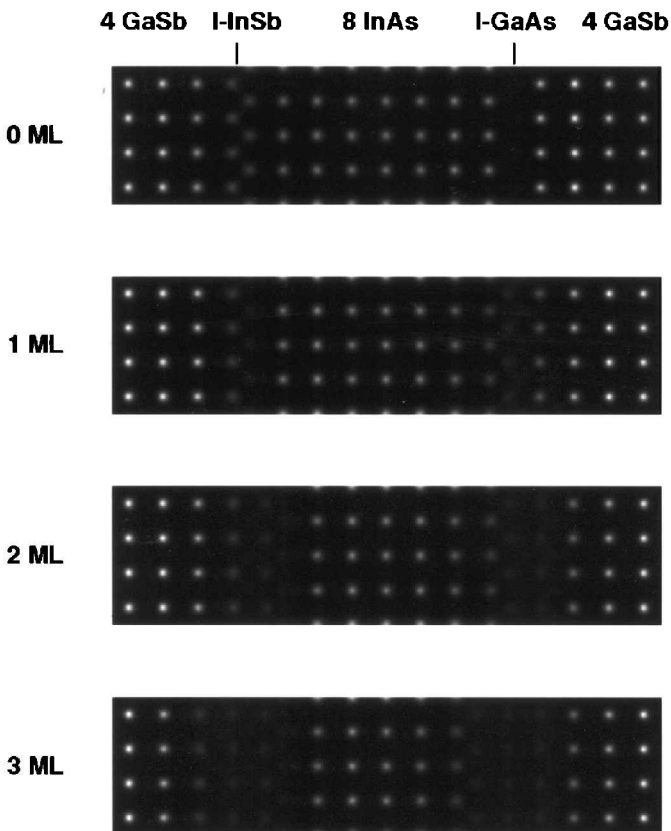
dark. At a defocus of 20 nm, we have the opposite effect: atomic columns corresponding to small atomic numbers (gallium and arsenic) appear dark; atomic columns corresponding to large atomic numbers (indium and antimony) appear bright, as shown in the simulation in fig. 8. This interpretation of the 60 nm defocus condition is analogous to that proposed by Ourmazd *et al.* (1990) in their study of $\text{Al}_x\text{Ga}_{1-x}\text{As}/\text{GaAs}$.

The results of multislice simulations of HRTEM images corresponding to the 20 nm defocus condition are shown in fig. 9. We simulated SL images with abrupt GaAs and InSb interfaces as well as those in which the interfaces were replaced by 1–3 ML of the composition $\text{In}_{0.5}\text{Ga}_{0.5}\text{As}_{0.5}\text{Sb}_{0.5}$ in order to mimic the contrast effects of 1 or 2 ML of interface disorder. Examples of the artificial unit cells that are the basis of these simulations are shown in fig. 10. By comparing these simulated images with experimental results, the degree of interfacial disorder can be estimated.

3.2. Quantitative image processing of HRTEM data

In order to make a quantitative assessment of the images recorded by HRTEM, we digitized portions of the negatives as 256×256 8-bit arrays using a charge-coupled device (CCD) camera. An example of such a digitized image, taken from an ion-milled specimen recorded at a defocus of 20 nm (InSb-bonded InAs/GaSb superlattice grown on $1 \mu\text{m}$ of GaSb on GaAs(100)) is shown in fig. 11(a). The digital filtering process begins with taking the 2D fast Fourier transform (FFT) of the recorded image, as shown in fig. 11(b). In order to digitize the image in such a way as to avoid the undersampling that leads to aliasing, we first need to know what sampling interval to use (i.e. the number of pixels per unit distance). According to the sampling theorem, imaging data would need to be sampled at twice the highest spatial frequency in order to prevent aliasing (Bracewell 1978). From the Fourier spectrum, it appears that highest spatial frequency is $\{420\}$. For InSb, the largest unit cell of the four III–V compounds involved in our study (lattice parameter, 0.64794 nm), d_{420} is 0.1488 nm. For GaAs, with the smallest unit cell in our study (lattice parameter, 0.56533 nm), d_{420} is 0.12641 nm. Even if we were to consider satellites of $\{420\}$ at $\{520\}$, we would have a value of $d_{520} = 0.104$ for GaAs. If we

Fig. 9



HRTEM simulations of [100]-oriented InAs/GaSb SL with 8 ML of InAs separated from 8 ML of GaSb by alternating GaAs and InSb interfaces. Simulations correspond to a defocus of 20 nm, a spherical aberration coefficient of 0.9 mm and an accelerating voltage of 300 kV. Interface widths in the simulations range from 0 ML (those completely devoid of roughness) to 1, 2 or 3 ML.

were to sample at twice the spatial frequency of GaAs{520}, we would find ourselves sampling at a rate of once every 0.052 nm (i.e. about twice every ångström). Because our CCD camera is sampling once every 0.025 nm (i.e. four times every ångström), there is no danger of undersampling.

From nonlinear imaging theory for the [001] zone axis, we know that only the {200} and {420} spatial frequencies (see fig. 6) contribute to the intensity of the {200} reflections (Thoma and Cerva 1991b). Therefore we multiply the FFT by a masking function (shown in fig. 11(c)) so that only the spatial frequencies near the {200} and {420} positions are present in the FFT (as shown in fig. 11(d)) and the filtered image (shown in fig. 11(e)). It should be noted that the vertical (i.e. perpendicular to a horizontal interface) extent of the spatial frequency bandwidth allowed by the mask is fairly large. We found that a large vertical value for the spatial frequency bandwidth was necessary in order to include sufficient Fourier components to allow the interface in the processed image to be abrupt. However, we limited the vertical

Fig. 10

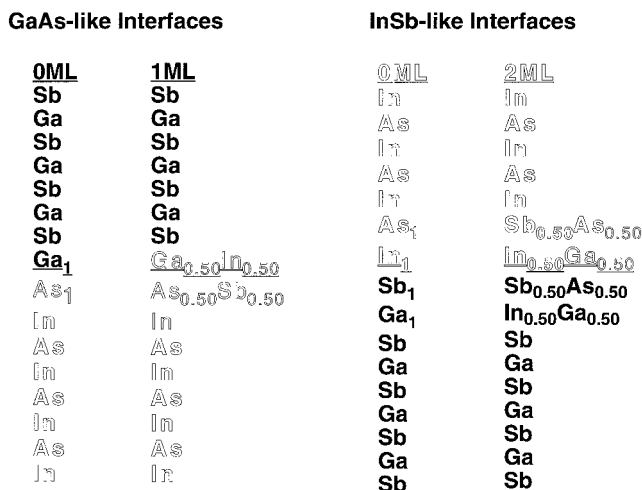


Diagram showing models for interfacial disorder. Here we show four examples: two different degrees of interfacial disorder for GaAs-like interfaces (0 and 1ML) and InSb-like interfaces (0 and 2ML). We substituted 1 ML of $\text{In}_{0.50}\text{Ga}_{0.50}\text{As}_{0.50}\text{Sb}_{0.50}$ for each 1 ML of interfacial disorder.

Fig. 11

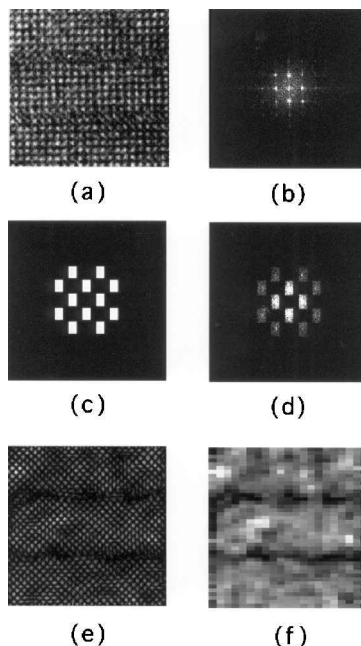


Image processing of HRTEM images of InAs-GaSb interfaces as described by Thoma and Cerva. (a) recorded image; (b) amplitude of FFT of image; (c) the mask for $\{200\}$ and $\{420\}$ spatial frequencies; (d) masked FFT; (e) filtered image obtained by inverse FFT of masked FFT; (f) resampling the filtered image which yields the final processed HRTEM image.

bandwidth so as to minimize the contribution of satellites of the $\{220\}$ spatial frequencies, which are not sensitive to the differences between the cation and anion scattering factors (Ourmazd *et al.* 1990).

In the filtered image, both cation and anion columns are present. This situation is, of course, different from the original image (recorded at a defocus of 20 or 60 nm) in which only one (either cation or anion) type of column is present. By removing the contribution of the $\{220\}$ reflections from the image, the spatial frequencies that allow cation and anion columns to be distinguished from one another are eliminated. Even though the filtered image in Fig. 11(e) is more sensitive to differences between anion and cation scattering factors than the recorded image shown in fig. 11(a), additional processing is still required. A plot of locally averaged $\{200\}$ intensity as a function of distance from the interface would be more useful in characterizing the extent of interfacial disorder. If we were to plot the intensity variations away from one interface (as in fig. 11(e)) we would obtain intensity oscillations due to the atomic columns. The problem of atomic-scale oscillations can be avoided by simply resampling the image so that we are only reading intensities from areas corresponding to a pair of anion–cation columns. For the 256×256 pixel image in fig. 11(f), the resampling area is 6×12 pixels, which corresponds to $0.15 \text{ nm} \times 0.3 \text{ nm}$ (i.e. one atomic column vertically by two atomic columns horizontally; essentially one cation and one anion column side by side). We chose to orient this sampling area laterally so that we would have one-atomic-layer resolution perpendicular to the interface. In this way we arrived at a processed image that is an intensity map for the compositionally sensitive $\{200\}$ reflections. Because the InSb and GaAs interfaces give rise to much smaller $\{200\}$ diffracted intensities than are excited in the InAs and GaSb layers in the SL, the processed image in fig. 11(f) shows much better definition of the interface width than the original recorded image in fig. 11(a).

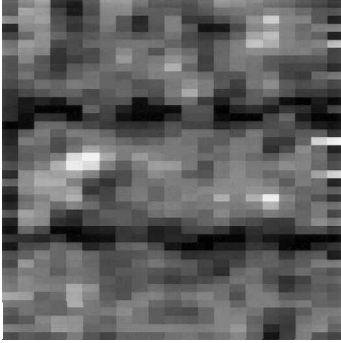
3.3. *The assessment of interfacial disorder via high-resolution transmission electron microscopy*

The difference between the processed HRTEM images of InSb-like and GaAs-like interfaces in SLs grown on a $1 \mu\text{m}$ GaSb buffer layer on GaAs(100) is shown in fig. 12. In fig. 13, we show processed images of SLs grown on a $1 \mu\text{m}$ InAs buffer layer on GaAs(100). The results of averaging several of these images of InAs–GaSb interfaces are shown in fig. 14. The quantification of simulated images that have undergone image processing is shown in fig. 15. Our interpretation of these images should, however, be viewed in the context of Raman spectroscopy results (i.e. that the interfaces are locally abrupt) (Bennett *et al.* 1993, Shanabrook *et al.* 1993, Shanabrook and Bennett 1994). Therefore we consider the interfacial disorder in these SLs to be principally due to interfacial roughness (Twigg *et al.* 1994).

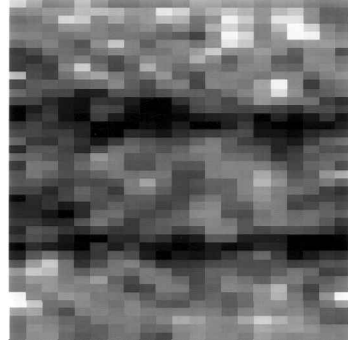
A comparison of the interface profiles in fig. 14 with the simulated profiles in fig. 15 suggests that the interfacial disorder (which we interpret as interfacial roughness) for SLs grown on a GaSb buffer layer is of the order of 1 ML for the InSb-like interface and 2 ML for the GaAs-like interface. The interface roughness for SLs grown on an InAs buffer is of the order of 2 ML for the InSb-like interface and 3 ML for the GaAs-like interface. From these results, it seems that not only is interface roughness greater for GaAs-like interfaces than for InSb-like interfaces but also the roughness is greater for SLs grown on an InAs buffer layer than for SLs grown on a GaSb buffer layer. For the $\text{Ge}_x\text{Si}_{1-x}$ system, a rougher surface occurs for films

Fig. 12

InSb bonds, GaSb buffer



GaAs bonds, GaSb buffer



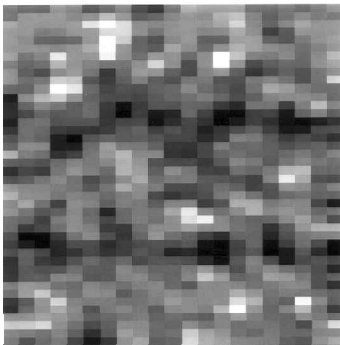
Processed HRTEM images of 8 ML InAs/12 ML GaSb SLs grown on GaSb buffer layers on GaAs(100) substrates. The InAs layer is in the middle with a GaSb layer on top and bottom, and the growth direction is from bottom to top. The InSb-like interfaces (on the left) have a roughness of 1 ML. The GaAs-like interfaces (on the right) have roughnesses of 2 ML.

under compression than under tension (Xie *et al.* 1994). Such may also be true in our system, since the GaSb SL layers are under compression when grown on an InAs buffer layer, whereas the InAs SL layers are under tension when grown on a GaSb buffer layer (Twigg *et al.* 1995a,b). These values of interface roughness are similar to those measured for InAs/GaSb superlattices by De Cooman *et al.* (1989) using dark-field transmission electron microscopy.

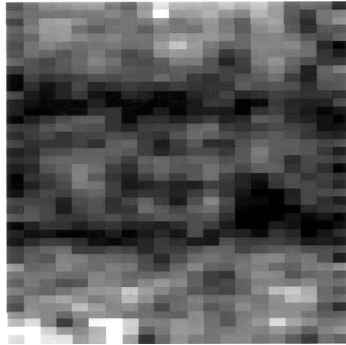
The large lattice mismatch of both GaSb and InAs with respect to a GaAs(100) substrate (7–8%) leads to threading dislocations in the GaSb or InAs buffer layer

Fig. 13

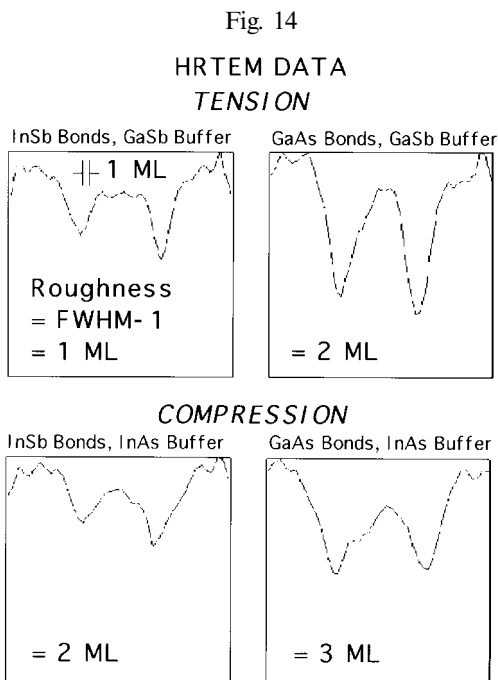
InSb bonds, InAs buffer



GaAs bonds, InAs buffer



Processed HRTEM images of 8 ML InAs/12 ML GaSb SLs grown on InAs buffer layers on GaAs(100) substrates. The InAs layer is in the middle with a GaSb layer on top and bottom, and the growth direction is from bottom to top. The InSb-like interfaces (on the left) have a roughness of 2 ML. The GaAs-like interfaces (on the right) have roughnesses of 3 ML.



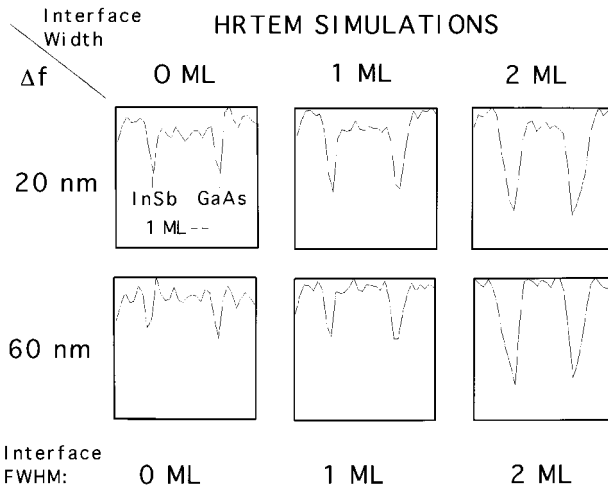
Intensity profiles derived from image processing of several images for each combination of interface type and buffer layer shown in figs. 12 and 13. The quantification scheme suggested in fig. 15 was used to determine the degree of interfacial roughness.

(Kang *et al.* 1994). Although the dislocation density in the SLs grown on a $1\ \mu\text{m}$ GaSb or InAs buffer layer is less than $10^7 \times \text{cm}^{-2}$, there is still the possibility that dislocations affect the surface and interface morphologies (Thibado *et al.* 1996). In order to rule out the possible effects of these dislocations on interfacial disorder, we also grew the SL on GaSb(100) substrates. Growing the SL on a GaSb substrate also allows us to prepare the HRTEM sample by cleaving, a process that results in a sample that is generally cleaner and better defined than a sample thinned by ion milling.

In fig. 16 we show a HRTEM image recorded from a cleaved specimen, at a defocus of 60 nm, where the thickness of the sample increases from right to left. There are two types of interface in this sample. The bottom interface is InSb-like; the top interface is GaAs-like. As was the case for InAs/GaSb SLs grown on a GaSb buffer layer on GaAs(100), the interface roughness was of the order of 1 ML for InSb-like interfaces and 2 MLs for GaAs-like interfaces. We estimate that the thinnest part of the sample shown in fig. 16 is 10 nm thick and the thickest part of the sample is 20 nm thick. Careful inspection of the processed image in fig. 16 reveals that the portion of the InSb-like interface defined by the left profile appears narrower than the portion of the interface defined by the right profile.

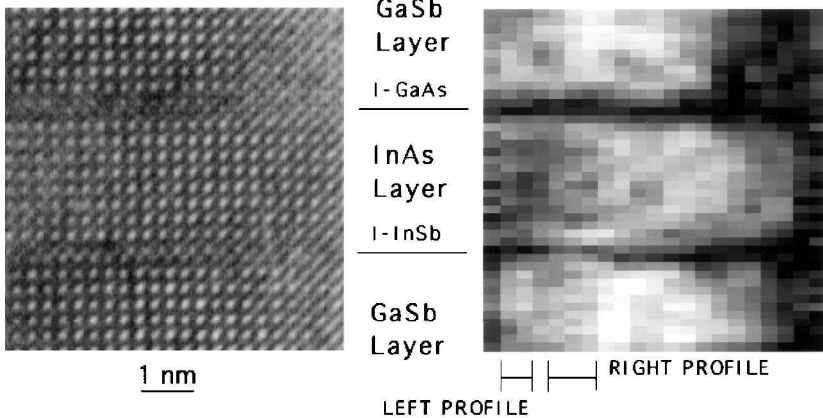
We make a quantitative comparison of the left and right profile regions of fig. 16 in fig. 17, where we plot the integrated intensities of the processed image (i.e. the intensity of the $\{200\}$ reflections) as a function of the distance from the interfaces for these two regions. The profile of left profile region of the InSb-like interface closely

Fig. 15



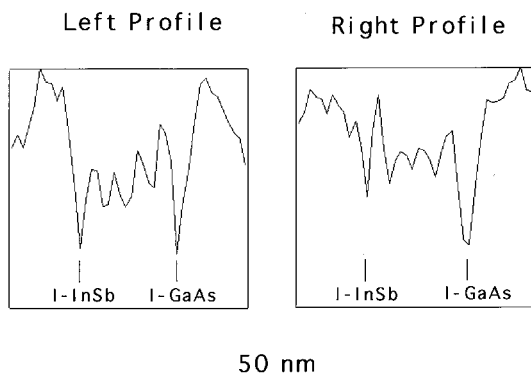
Intensity profiles derived from image processing of multislice simulations for two defocus values (20 and 60 nm) and three values of interface width (0, 1 and 2 ML). Note that the full width at half-maximum (FWHM) of the profiles increases with increasing interface width. The interface width is attributed to interface roughness for the InAs/GaSb SLs grown in this study.

Fig. 16



To the left is a HRTEM image of cleaved specimen taken from an InAs/GaSb SL grown on a GaSb buffer layer and GaSb(100) substrate. The defocus value is 60 nm. The processed image on the right, taken from the HRTEM image on the left maps intensities associated with $\{200\}$ reflections. Note that the left portion of the InSb interface (left profile) is more abrupt than the right portion (right profile) of the InSb interface.

Fig. 17



The $\{200\}$ intensity profiles from the processed image in fig. 16. The left profile is taken from an average of the two columns allotted to this profile in fig. 16. The right profile is taken from an average of the three columns allotted to this profile in fig. 16. Note that in each case the InSb-like interface is more abrupt than the GaAs-like interface. Also, the InSb-like interface in the left profile is more abrupt than the InSb-like interface in the right profile.

resembles the simulated profile in fig. 15 for an abrupt (0 ML wide) InSb interface recorded at a defocus of 60 nm. The InSb-like interface in the left portion is then abrupt. The right profile of the InSb-like interface in fig. 17 resembles a rougher (1 ML wide) InSb-like interface recorded at a defocus of 60 nm (as also shown in fig. 16). The abrupt InSb-like interface in the image corresponds to a region of the sample where the imaging electrons of the HRTEM traverse a 15 nm path over a portion of the specimen devoid of steps or terraces. The existence of such an abrupt InSb-like interfacial region would not be possible if significant interdiffusion had occurred. The rougher portion of the InSb-like interface corresponds to a region where steps and terraces are present. There is also evidence for the existence of a locally abrupt GaAs-like interface in the left profile of the processed image in fig. 16 (as shown in the left profile in fig. 17).

It should also be noted that interfacial disorder in InAs/GaSb SLs grown by MOVPE has been investigated by Murgatroyd *et al.* (1995). Their HRTEM study found the frequent occurrence of step bunching. Between steps, however, the interface frequently appeared abrupt, strongly suggesting that interfacial disorder is principally the product of interfacial roughness rather than interfacial diffuseness.

§ 4. INTERFACIAL MORPHOLOGY

In order to characterize interfacial disorder in InAs/GaSb heterostructures further, we performed a complimentary study utilizing *in-situ* STM on a number of interfacial surfaces in plan view. With plan-view STM, both the 3D morphology and the atomic-scale structure of the evolving epitaxial interfaces can be observed directly. The growth program used for the cleaved HRTEM samples (grown on a GaSb(100) substrate) described above was used for these samples as well. However, after the samples were grown up to the point of interest, an appropriate anion soak was used to terminate the growth. The sample was then quenched to room tempera-

ture in the absence of any flux and transferred under ultrahigh vacuum to the surface analysis chamber. STM images were acquired with a constant current of 0.1 nA and sample bias between -1.8 and -2.2 V. In order to minimize any possible effects of surface contamination on the superlattice morphology, after examination by STM, each interface was buried under at least 0.5 μm of GaSb and the superlattice was regrown up to the next interface of interest (Thibado *et al.* 1995).

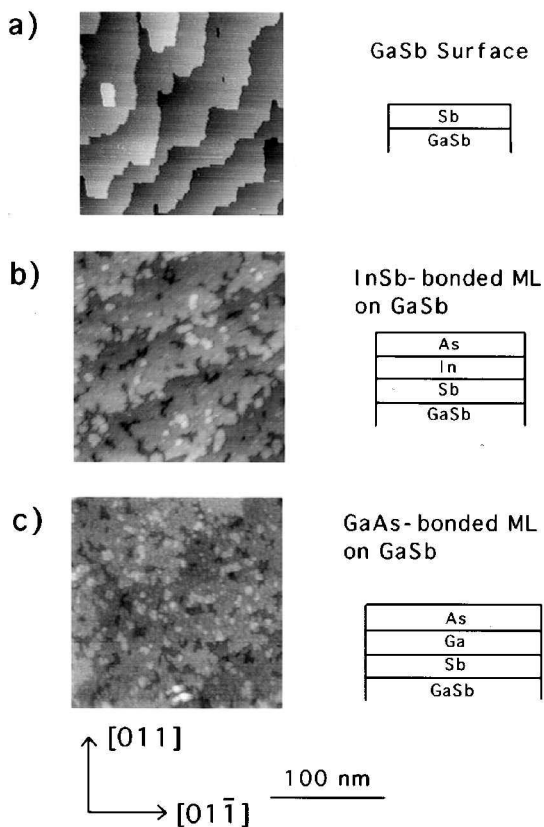
A STM image of the surface of a typical GaSb buffer layer grown on a GaSb(100) substrate is shown in fig. 18(a). The surface is antimony terminated and consists of large, atomically smooth terraces (about 50 nm wide) separated by monolayer-height (0.3 nm) steps, with very few adatom or vacancy islands. This surface appears to be close to thermodynamic equilibrium, so that the average terrace width is determined by the misorientation of the sample with respect to (100). (Some regions of the sample may have larger terraces than others owing to local variation in the orientation due to polishing.) Atomically resolved images on each terrace (not shown) reveal the antimony-terminated 1×3 surface reconstruction, consistent with RHEED. The stability of the $[011]$ -oriented rows of antimony dimers inherent to this reconstruction give the terrace edges their characteristically straight $[011]$ -oriented and jagged $[0\bar{1}1]$ -oriented edges. Thin GaSb films (8 ML) grown at 400°C within the superlattice have a very similar surface structure to the GaSb buffer (atomically smooth terraces with few vacancy or adatom islands), but with more rounded terrace edges. Our *in situ* STM characterization of the GaSb-InAs interfaces will focus on the disorder due to roughness, defined as the number of additional monolayers present on each terrace at the completion of interface growth. It can be characterized on any length scale, but we shall focus on two: firstly the total roughness on each substrate terrace, a good indication of the overall roughness associated with the growth; secondly the roughness within a typical line 20 nm long oriented in the $\langle 100 \rangle$ direction, a sampling comparable with that viewed by HRTEM. The roughness on the clean GaSb(100) surfaces, as defined here, is 0 ML on both length scales.

The addition of an interface layer to a GaSb(100) 1×3 surface causes significant changes in the surface morphology. Following the growth of an arsenic terminated InSb interface (fig. 18(b)), small vacancy islands 1 ML deep and adatom islands 1 ML high (10 nm diameter) are observed on each terrace, giving the terraces a roughness of 2 ML. Owing to the low density of these features, the typical roughness on the length scale sampled in HRTEM (20 nm) is only 1 ML (i.e. along this sampling length either a vacancy or adatom island would typically be encountered).

Following the deposition of an arsenic-terminated GaAs surface on GaSb(100) (corresponding to a GaAs-like interface in the SL) (fig. 18(c)) a greater degree of roughening is observed. Small vacancy and adatom islands are now observed on each terrace, similar to the InSb-like interface, but with approximately equal areas and twice the density; this surface has a terrace roughness of 2 ML. The surface roughness averaged over 20 nm along a $\langle 001 \rangle$ direction, as occurs in HRTEM imaging, is also 2 ML. The GaAs surface is also noticeably rougher on the atomic scale than the InSb interface.

The arsenic-terminated InAs starting surface consists of 8 ML of InAs grown on a GaSb(100) buffer layer. (Since the InAs layer is well under the critical layer thickness, it is coherently strained.) As shown in fig. 19(a), this surface consists of large terraces with very few islands or pits, similar to the GaSb(100) starting surface

Fig. 18

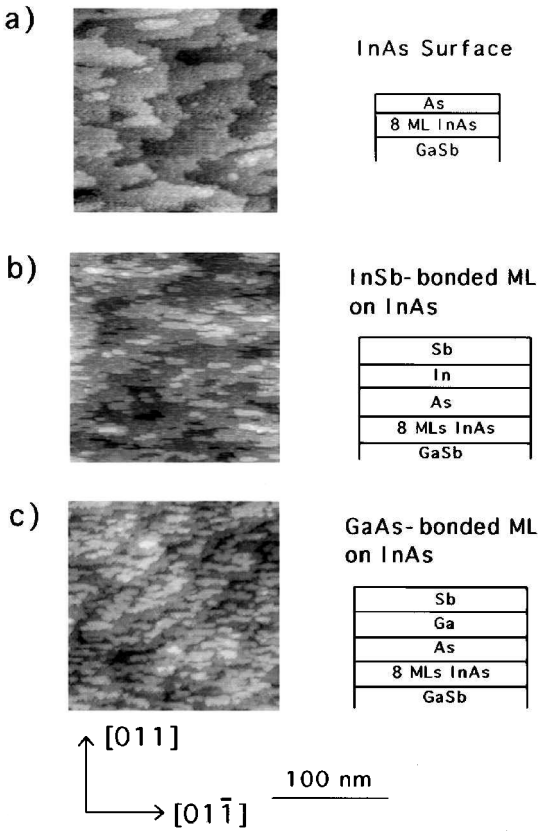


STM images of surfaces corresponding to various internal interfaces occurring in the first period of an InAs/GaSb SL grown on a GaSb(100) buffer layer and substrate, where the images were acquired with a constant current of 0.1 nA and sample biases between -1.8 and -2.2 V: (a) GaSb(100) buffer layer; (b) InSb-like interface on GaSb; (c) GaAs-like interface on GaSb. The topmost layers at each surface are indicated in schematic diagrams to the right of the images.

(terrace roughness averaged over 20 nm is 0 ML), but with terrace fingers elongated along the [011] direction; there is also much more atomic-scale disorder. In contrast with the clean GaSb surfaces, the clean InAs surfaces do not appear to be as close to thermodynamic equilibrium. Although the atomic-scale structure is not well ordered, the finger-like shape of the terrace edges indicates that there is some reconstruction-related local order (consistent with RHEED); the [011]-oriented row-like structure of arsenic-terminated InAs(100) 2×4 promotes growth along this direction.

The addition of an arsenic-terminated InSb layer (corresponding to an InSb-bonded interface in the SL) to the strained InAs film further roughens the surface (fig. 19(b)), with many large (30–50 nm) elongated adatom islands appearing along with some generally smaller elongated vacancy islands (giving a terrace roughness of 2 ML). The terrace edges are also more jagged, which can be attributed to the growth

Fig. 19



STM images of surfaces corresponding to various internal interfaces occurring on a strained InAs(100) epitaxial layer 8 ML thick on GaSb: (a) arsenic-terminated InAs layer; (b) InSb-like interface on InAs; (c) GaAs-like interface on InAs. The topmost layers at each surface are indicated in schematic diagrams to the right of the images.

mode whereby elongated islands are incorporated incompletely into the terrace edges. The asymmetric nature of the surface features is a further indication of a strong directional anisotropy in the growth of indium on the InAs surface. This directional anisotropy has also been seen in cross-sectional scanning tunnelling microscopy (XSTM) of InAs/GaSb SLs (Lew *et al.* 1997). Although this surface appears rougher than the InSb–GaSb interface surface, the roughness averaged over 20 nm is also approximately 1 ML (owing to the larger island size).

The roughest surface examined was the arsenic-terminated GaAs-like interface on InAs (fig. 19(c)), a surface with a very high density of interconnected islands. The islands are elongated in the $[011]$ direction as in the InSb/InAs case, but with noticeably rounder edges. Note that many islands have clearly become attached to the terrace edges, making it difficult to discern the underlying substrate terraces. However, based on the typical terrace width on the InAs surface, we estimate the roughness per terrace to be 3 ML (four layers are present, but the fourth layer is sparse). We find that a line 20 nm long along $\langle 001 \rangle$ would typically encompass

three layers on this surface, corresponding to a roughness of 2 ML on this length scale.

Under our growth conditions, we find that the interfacial surfaces on GaSb are smoother than those on strained InAs, and that the InSb-like interfaces are generally smoother than GaAs-like interfaces for both surfaces (a roughness averaged over 20 nm of 1 ML as against 2 ML). These observations are consistent with the widths of identically grown interfaces measured with HRTEM. Most significantly, the roughness that we observe on the 20 nm length scale, associated with the vacancy and adatom island shapes and size distributions, completely accounts for the interface widths observed via HRTEM, as shown in fig. 14.

§ 5. DISCUSSION

The morphology of the interfacial surface is influenced by the surface kinetics as well as by the equilibrium configuration of the surface. We have noted that the GaAs bond is significantly stronger than the InSb bond. From the standpoint of kinetics, therefore, we expect diffusion to proceed more quickly over an InSb-bonded surface than a GaAs-bonded surface. As a result, kinetics may leave an InSb-like surface smoother than a GaAs-like surface. For a surface that has reached equilibrium (i.e. where kinetics have had sufficient opportunity to run their course) we would also expect for an InSb-bonded surface to be smoother than a GaAs-bonded surface. The equilibrium configuration of a surface with a large energy per unit area, such as the GaAs-like surface, may not be a flat surface; instead the equilibrium configuration may be that of GaAs islands on a GaSb or InAs surface. It is more likely, of course, for a surface with a low energy per surface area, such as an InSb-like surface to assume a planar equilibrium configuration.

The close correspondence between the degree of interface roughness (as determined via HRTEM) and the roughness of the interfacial surface for thin GaSb or InAs layers grown on a GaSb(100) substrate (as determined by *in-situ* STM) suggests that the morphology of the interfacial surface is primarily responsible for the roughness of the interface. The conclusion is limited, of course, to the MEE growth procedure used here, where anion exchange reactions are prevented by the deposition of individual cation monolayers. This absence of exchange reactions in MEE-grown InAs/GaSb SLs is confirmed by the results of Raman scattering experiments.

Although disorder in our MEE-grown interfaces appears to assume the form of interfacial roughness, there is evidence for the presence of interfacial diffuseness or exchange reactions in the study of InAs/GaSb interfaces using XSTM, by Feenstra *et al.* (1994b). Their observations indicate that the InAs-on-GaSb interface has more intermixing than the GaSb-on-InAs interface does. This was found to be the case for anion soaks of both Sb₂ and As₂ at the interfaces. These observations were rationalized in terms of an antimony-terminated surface having a lower free energy than an arsenic-terminated surface, resulting in an exchange of antimony and arsenic when InAs is grown on GaSb. When GaSb was grown on InAs, no exchange was thought to occur. The disorder in the InAs/GaSb interfaces studied by Feenstra *et al.* was attributed to exchange reactions, as might be expected from the nature of the MBE growth procedure used in growing their samples. In the study by Feenstra *et al.*, the interfaces were established using anion soaks alone, rather than an anion soak that is preceded or followed by a cation monolayer (as in our MEE procedure). It is interesting to note that the tendency for more ordered GaSb-on-InAs interfaces

(compared with InAs-on-GaSb interfaces) has also been observed by Lyapin *et al.* (1994, 1995) via Raman spectroscopy for GaAs-like interfaces in SLs grown by MOVPE.

Both *in-situ* STM and HRTEM measurements of our InAs–GaSb interfaces, indicate that InSb-like interfaces are smoother than GaAs-like interfaces, as would be expected from kinetic or thermodynamic arguments. Although the growth procedure used in growing the samples analysed by Feenstra *et al.* differ from our MEE growth procedure, it is still important to note that Feenstra *et al.* (1994a) noticed no significant difference in InSb-like and GaAs-like interfaces with respect to interfacial disorder. It is also conceivable that the apparent similarity of InSb-like and GaAs-like interfaces in XSTM may result from the morphology of the (110) zincblende surface. Owing to the zincblende structure of a (110) surface, only every other (001) bilayer plane is exposed on the (110) surface. Therefore the cleavage surface may reveal the top layers above and below an interface rather than the interface itself. It is therefore conceivable that XSTM is not able to resolve the difference between 1 and 2 ML of interface roughness. This morphological artefact may explain why Feenstra *et al.* do not report any difference in interface roughness between GaAs-like and InSb-like interfaces in InAs/GaSb SLs.

The nature of interfacial disorder in our SLs is also suggested by the tendency for disorder to be greater for SLs grown in tension and less for SLs grown under compression. There is experimental evidence that a surface or interface grown under compression is rougher than when grown under tension (Twigg *et al.* 1995a,b, Xie *et al.* 1995). This difference between tension and compression may be rationalized in terms of dimer bonds that are under particularly great tensile strain at a terrace step (Xie *et al.* 1995). In InAs/GaSb SLs, GaSb layers are under compression when grown on an InAs buffer layer, whereas InAs layers are under tension when grown on a GaSb buffer layer. Therefore, one might expect an InAs/GaSb SL grown on a GaSb buffer layer to have less interface roughness than an InAs/GaSb SL grown on an InAs buffer layer.

§6. CONCLUSIONS

We have used a number of experimental techniques to determine the nature of interfacial disorder in InAs/GaSb SLs. From X-ray diffraction, we know that overall control of composition at the interfaces is good (Bennett *et al.* 1993). From Raman spectroscopy we have found that the nominally InSb-like interfaces have an As_xSb_{1-x} anion composition where $x < 0.1$ (Shanabrook *et al.* 1993). The reproducibility of the Raman spectra for SLs grown with GaAs-like interfaces suggests that GaAs-like interfaces are also well controlled. These results also suggest that these heteroepitaxial interfaces are locally abrupt. The MBE technique used in growing these interfaces, MEE, deposits alternating cation and anion layers, with the less mobile cation monolayer isolating the adjacent anion layers so as to minimize intermixing or exchange reactions.

Our HRTEM imaging experiments have found that there is a degree of disorder in InAs/GaSb interfaces grown on GaSb buffer layers. This degree of disorder was found to be of the order of 2 MLs for GaAs-like interfaces and 1 ML for InSb-like interfaces. The Raman spectroscopy results indicate that intermixing occurs for less than 10% of the atoms forming an InSb-like interface, a result that is incompatible with a full 1 ML of interfacial disorder, unless most of this disorder is ascribed to a cause other than intermixing. The HRTEM and Raman results are, however, con-

sistent with the contention that InSb-like interfaces are locally abrupt, suggesting that interfacial disorder assumes the guise of island formation (resulting in interfacial roughness) rather than interdiffusion or exchange reactions (resulting in diffuse interfaces). Indeed, small regions of atomically abrupt interfaces have been observed in our HRTEM study of InAs/GaSb SLs with InSb-like and GaAs-like interfaces (Twigg *et al.* 1995a,b). We have also studied the interfaces for InAs/GaSb SLs grown on InAs buffers. These interfaces were found to exhibit a greater degree of roughness than those grown on GaSb buffers. Again, GaAs-like interfaces proved rougher than the InSb-like interfaces. From the results of HRTEM imaging experiments, it appears that the interfaces may be less rough when grown on a GaSb buffer layer (as compared to an InAs buffer layer) because the SL is grown under tension instead of compression.

Despite our progress in achieving a better understanding of interfacial disorder in InAs/GaSb heterostructures, a host of unanswered questions remain. How much smoother can the interfacial surface become if the newly arrived adatoms have sufficient time to diffuse? Is there a danger of intermixing during surface diffusion? How is the surplus or deficit in the number of anions terminating reconstructed surfaces compensated during epitaxial growth? What is the role of steps in anion exchange reactions? It is conceivable that these questions can eventually be answered, especially by a systematic *in-situ* STM, XSTM and HRTEM study of InAs–GaSb interfaces and surfaces prepared under a wide range of growth conditions.

ACKNOWLEDGEMENTS

This work was sponsored by the Office of Naval Research and the Naval Research Laboratory—National Research Council Post-doctoral Fellowship Program (P.M.T.). We thank Larry Ardis for expert technical assistance. We also thank Jim Waterman, Bob Wagner and Ming-Jey Yang for their insights regarding narrow-bandgap materials and heterostructures.

REFERENCES

- BAUER, E., 1958, *Z. Kristallogr.*, **110**, 372.
 BENNETT, B. R., SHANABROOK, B. V., and MAGNO, R., 1996, *Appl. Phys. Lett.*, **68**, 958.
 BENNETT, B. R., SHANABROOK, B. V., and WAGNER, R. J., DAVIS, J. L., Waterman, J. R., 1993, *Appl. Phys. Lett.*, **63**, 949.
 BRACEWELL, R. N., 1978, *The Fourier Transform and its Applications*, second edition (New York: McGraw-Hill).
 BRESSLER-HILL, V., LORKE, A., VARMA, S., PETROFF, P. M., POND, K., and WEINBERG, W. H., 1994, *Phys. Rev. B*, **50**, 8479.
 CHEN, X., F. WU, F., ZHANG, Z., and LAGALLY, M. G., 1994, *Phys. Rev. Lett.*, **73**, 850.
 CHOW, D. H., MILES, R. H., and HUNTER, A. T., 1992, *J. vac. Sci. Technol. B*, **10**, 888.
 COPEL, M., REUTER, M. C. KAXIRAS, E., and TROMP, R. M., 1989, *Phys. Rev. Lett.*, **63**, 632.
 DE COOMAN, B. C., CARTER, C. B., WICKS, G. W., TANOUÉ, T., and EASTMAN, L. F., 1989, *Thin Solid Films*, **170**, 49.
 FEENSTRA, R. M., COLLINS, D. A., and MCGILL, T. C., 1994a, *Superlattices Microstruct.*, **15**, 215.
 FEENSTRA, R. M., COLLINS, D. A., TING, D. Z.-Y., WANG, M. W., and MCGILL, T. C., 1994b, *Phys. Rev. Lett.*, **72**, 2749.
 FRANKLIN, G. E., RICH, D. H., SAMSAVARR, A., HIRSHORN, E. S., LEIBSLE, F. M., MILLER, T., and CHIANG, T.-C., 1990, *Phys. Rev. B*, **41**, 12 619.
 GAMMON, D., SHANABROOK, B. V., and KATZER, D. S., 1991, *Phys. Rev. Lett.*, **67**, 1547.

- GRIGORIEFF, N., CHERNS, D., YATES, M. J., HOCKLY, M., PERRIN, S. D., and AYLETT, M. R., 1993, *Phil. Mag.*, **68**, 121.
- HELLER, E. J., ZHANG, Z. Y., and LAGALLY, M. G., 1993, *Phys. Rev. Lett.*, **71**, 743.
- HOFFMAN, C. A., MEYER, J. R., BARTOLI, F. J., and WANG, W. I., 1993, *Phys. Rev. B*, **48**, 1959.
- HORIKOSHI, Y., KAWASHIMA, M., and YAMAGUCHI, H., 1986, *Jap. J. Appl. Phys.*, **25**, L868.
- KANG, J. M., NOUAOURA, M., LASSABATERE, L., and ROCHER, A., 1994, *J. Cryst. Growth*, **143**, 115.
- LEW, A. Y., ZUO, S. L., YEW, E. T., and MILES, R. H., 1997, *Appl. Phys. Lett.*, **70**, 75.
- LYAPIN, S. G., KLIPSTEIN, P. C., MASON, N. J., and WALKER, P. J., 1994, *Superlattices Microstruct.*, **15**, 499; 1995, *Phys. Rev. Lett.*, **74**, 3285.
- MILES, R. H., CHOW, D. H., SCHULMAN, J. N., and MCGILL, T. C., 1990, *Appl. Phys. Lett.*, **57**, 801.
- MOISON, J. M., HOUZAY, F., BARTHE, F., GERARD, J. M., JUSSERAND, B., MASSIES, J., and TURCO-SANDROFF, F. S., 1991, *J. Cryst. Growth*, **111**, 141.
- MURGATROYD, I. J., MASON, N. J., WALKER, P. J., and BOOKER, G. R., 1995, *Microscopy of Semiconducting Materials*, Institute of Physics Conference Series No. 146 (Bristol: Institute of Physics), pp. 353–356.
- OURMAZD, A., BAUMANN, F. H., BODE, M., and KIM, Y., 1990, *Ultramicroscopy*, **34**, 237.
- OURMAZD, A., TAYLOR, D. W., CUNNINGHAM, J., and TU, C. W., 1989, *Phys. Rev. Lett.*, **62**, 933.
- PRIESTER, C., and LANNOO, M., 1995, *Phys. Rev. Lett.*, **75**, 93.
- SCHMITZ, J., WAGNER, J., FUCHS, F., HERRES, N., KOIDL, P., and RALSTON, J. D., 1995, *J. Cryst. Growth*, **150**, 858.
- SELA, I., SAMOSKA, L. A., BOLOGNESI, C. R., GOSSARD, A. C., and KROEMER, H., 1992, *Phys. Rev. B*, **46**, 7200.
- SHANABROOK, D. B., and BENNETT, B. R., 1994, *Phys. Rev. B*, **50**, 1695.
- SHANABROOK, B. V., BENNETT, B. R., and WAGNER, R. J., 1993, *Phys. Rev. B*, **48**, 17172.
- SHANABROOK, B. V., WATERMAN, J. R., DAVIS, J. L., and WAGNER, R. J., 1992, *Appl. Phys. Lett.*, **61**, 2338.
- SMITH, D. L., and MAIHIOT, C., 1987, *J. appl. Phys.*, **62**, 2547.
- SNYDER, C. W., ORR, B. G., and MUNEKATA, H., 1993, *Appl. Phys. Lett.*, **62**, 46.
- STADELMANN, P., 1987, *Ultramicroscopy*, **21**, 131.
- THIBADO, P. M., BENNETT, B. R., TWIGG, M. E., SHANABROOK, B. V., and WHITMAN, L. J., 1995, *Appl. Phys. Lett.*, **67**, 3578; 1996, *J. vac. Sci. Technol. A*, **14**, 885.
- THOMA, S., and CERVA, H., 1991a, *Ultramicroscopy*, **35**, 77; 1991b, *ibid.*, **38**, 265.
- TUTTLE, G., KROEMER, H., and ENGLISH, J. H., 1990, *J. appl. Phys.*, **67**, 3032.
- TWIGG, M. E., BENNETT, B. R., and SHANABROOK, B. V., 1995a, *Appl. Phys. Lett.*, **67**, 1609; 1995b, *Microscopy of Semiconducting Materials*, Institute of Physics Conference Series No. 146 (Bristol: Institute of Physics), pp. 349–352.
- TWIGG, M. E., BENNETT, B. R., SHANABROOK, B. V., WATERMAN, J. R., DAVIS, J. L., and WAGNER, R. J., 1994, *Appl. Phys. Lett.*, **64**, 3476.
- WANG, M. W., COLLINS, D. A., MCGILL, T. C., GRANT, R. W., and FEENSTRA, R. M., 1995, *J. vac. Sci. Technol. B*, **13**, 1689.
- WARWICK, C. A., JAN, W. Y., and OURMAZD, A., 1990, *Appl. Phys. Lett.*, **56**, 2666.
- WATERMAN, J. R., SHANABROOK, B. V., WAGNER, R. J., YANG, M. J., DAVIS, J. L., and OMAGGIO, J. L., 1993, *Semicond. Sci. Technol.*, **8**, S106.
- XIE, Y. H., GILMER, G. H., ROLAND, C., SILVERMAN, P. J., BURATTO, S. K., CHENG, J. Y., FITZGERALD, E. A., KORTAN, A. R., SCHUPPLER, S., MARCUS, M. A., and CITRIN, P. H., 1994, *Phys. Rev. Lett.*, **73**, 3006.
- YANO, M., YOKOSE, H., IWAI, Y., and INOUE, M., 1991, *J. Cryst. Growth*, **111**, 609.